Article

Leveraging computational tools to understand the triptolide-XPB interaction

David Gorrie [1*]

[1] Department of Biomedical Sciences, University of California Riverside, Riverside, CA, 92521, USA
* Correspondence: david.gorrie@email.ucr.edu

Abstract: Triptolide is a natural product isolated from a traditional Chinese medicinal plant for treating rheumatoid arthritis and other autoimmune diseases. Triptolide displays diverse bioactivities, including anti-inflammation, immunosuppression, anti-cancer, etc. Triptolide was reported to crosslink with the residue Cys342 of human XPB (HsXPB), a DNA helicase required for transcription and DNA repair. This interaction inhibits XPB's ATPase activity. Here, we report that triptolide specifically inhibits the ATPase activity of HsXPB but has no impact on its archaeal homologs, indicating that triptolide's effect on HsXPB is not conserved among XPB homologs. Computational docking further confirmed this, which showed that the predicted triptolide binding sites have different distribution patterns among HsXPB and its archaeal homologs. Computational modeling revealed that crosslinking of triptolide with Cys342 of HsXPB allows triptolide to occupy the positions of the β- and γ-phosphate of adenosine triphosphate (ATP) at the ATP binding site, therefore providing a barrier to ATP binding and hydrolysis by HsXPB.

Keywords: cancer, natural product, immunosuppression, anti-inflammatory, triptolide, XPB, docking analysis.

1. Introduction

Triptolide is a natural chemical isolated from the extract of the Chinese medicinal plant *Tripterygium wilfordii* Hook F (TwHF) [1], generally called Lei Gong Teng (Thunder God Vine). TwHF has been historically used to effectively treat rheumatoid arthritis and other autoimmune diseases [2-4]. Since its isolation in 1972 [1], triptolide has been reported to have an impressive spectrum of bioactivities, including anti-inflammation, antiproliferation, immunosuppression, anticancer, etc. [2-6]. At the molecular level, triptolide affects several transcription factors of different pathways and inhibits the overall mRNA synthesis [7,8]. Most recently, triptolide was reported to directly interact with XPB, a DNA helicase in the general transcription factor TFIIH complex, and covalently bind with the residue Cys342 of HsXPB to inhibit the ATPase activity of XPB [9]. However, this interaction was reported to have no impact on the helicase activity of HsXPB, which usually requires ATP binding and hydrolysis. XPB plays a key role in transcription initiation mediated by RNA polymerase II and in creating a repair bubble during nucleotide excision repair (NER), a significant DNA repair pathway that fixes various DNA lesions (including UV light-induced DNA damage) that disturb the DNA helical structure [10,11]. Therefore, the inhibitory binding of triptolide to XPB leads to the inhibition of both transcription and NER, likely the primary reason for the broad and diverse effects of triptolide on cell biology. If not quickly repaired, any DNA damage could cause mutations and genomic instability, leading to various diseases and even cancer. In fact, inherited XPB mutations are associated with a high risk of skin cancer and sunlight sensitivity, as well as childhood diseases xeroderma pigmentosum (XP), Cockayne syndrome (CS), and trichothiodystrophy [10]. It is a valuable strategy to target DNA damage response and repair pathways for cancer therapy [12]. Interestingly, DNA damage, often through covalent modification, is both a cause of cancer and a common strategy to induce cancer cell death.

Triptolide is a diterpene tri-epoxide molecule with three adjacent epoxide groups (Fig. 1). Although triptolide displays impressive clinical effects, it has poor water solubility and severe toxicity [4,13]. To conquer these shortcomings, numerous triptolide derivatives have been synthesized to study the structure-activity relationship (SAR) of triptolide and the mechanism of its action [2,14-16]. Among the four potentially reactive groups of triptolide (the butenolide moiety in ring D or one of the three epoxide groups, see Figure 1), only the 12,13-epoxide of triptolide was reported to mediate the covalent crosslink with the residue Cys342 of HsXPB [9]. Residue Cys342 is next to the Walker A motif (343GAGKS347), the ATP binding site conserved among all XPB homologs [9].

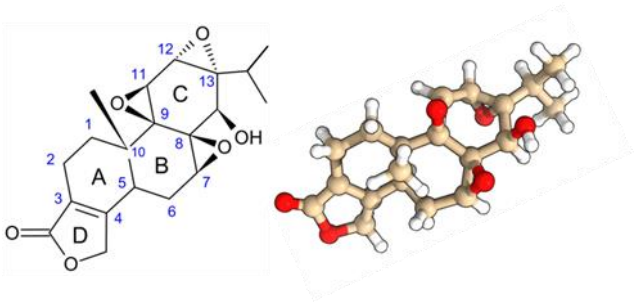

Figure 1. Chemical structure of triptolide.

To understand triptolide's interaction with XPB at the molecular level, we report here the results from computational docking of triptolide to HsXPB and its archaeal homologs from *Archaeogloubus fulgidus* (AfXPB) and *Sulfurisphaera tokodaii* (conventionally named StXPB2), together with the impacts of triptolide on the ATPase activity of these XPB enzymes.

2. Results and Discussion

2.1 Triptolide inhibits ATP hydrolysis by HsXPB but not archaeal XPB homologs

Triptolide was reported to inhibit the DNA-dependent ATPase activity of HsXPB by crosslinking with the residue Cys342 [9]. Since Cys342 is next to the Walker A motif (343GAGKS347), it is possible that the binding pocket of triptolide overlaps with the ATP binding. If this is true, triptolide could also inhibit the ATPase activity of XPB homologs. To test this hypothesis, we investigated the impact of triptolide on HsXPB and archaeal XPB homologs AfXPB and StXPB2 by my bespoke, in-house ATPase assay [17]. HsXPB was prepared as an XPB-p52-p8 trimer from insect cell culture because XPB alone is not stable as a recombinant protein.

We first examined the rate of ATP hydrolysis by HsXPB (Fig.2). In the absence of triptolide, we determined the maximum rate of reaction (Vmax) when 50 nM HsXPB was saturated with substrate ATP at 37 ^{0}C to be 2.21 μM [phosphate]/Minute. The k_{cat} was calculated to be 44.2 per minute. Based on the ATP hydrolysis velocity plots (Fig. 2B), we estimated the Michaelis constant (Km) (the substrate concentration at which the reaction rate is half of the maximum rate) for ATP hydrolysis by HsXPB to be 1.08 mM [ATP]. In the presence of 2.5 μM triptolide, the V_{max} of ATP hydrolysis by HsXPB was reduced to 0.75 μM [phosphate] /Minute. The k_{cat} was calculated to be 15.0 per minute. These results demonstrated that triptolide significantly inhibited the ATP hydrolysis by HsXPB, consistent with published results [8,9]. The K_m value changed to 0.55 mM [ATP] in the presence of 2.5 μM triptolide.

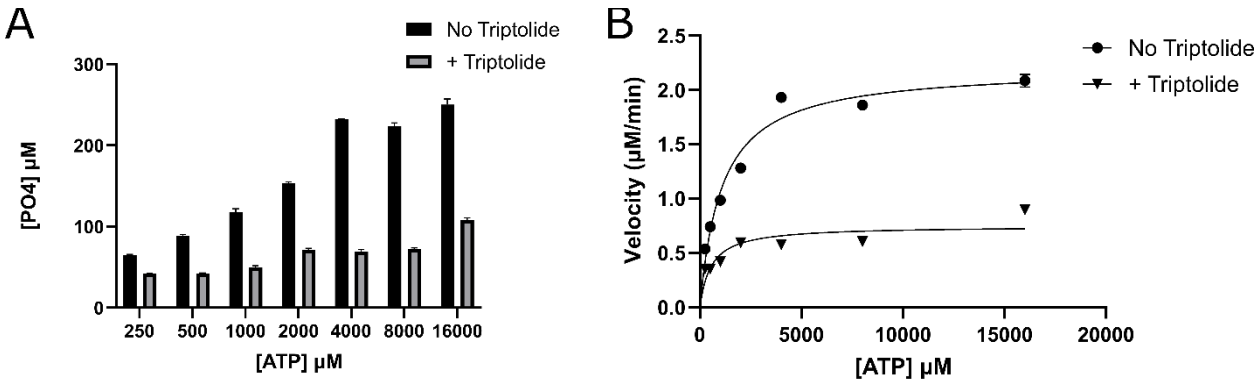

Figure 2. Triptolide inhibits the ATP hydrolysis by HsXPB**. A:** Phosphate produced from ATP hydrolysis by 0.050 μM HsXPB in the presence and absence of 2.50 μM triptolide at various ATP concentration ranging from 250 to 1600 μM. Data are mean ± standard deviation from triplicate measurements performed at 37 ^{0}C for 2 hours as described in the Methods except ssDNA oligomer is replaced by a bubble DNA of 0.375 μM as shown.

```
5'- GACAGGCTCACACGTTACGTTGCGCACGGC -3'
    ||||||||||||        ||||||||||||
3'- CTGTCCGAGTGTTGCCGCTAACGCGTGCCG -5'
```

Triptolide was prepared in DMSO, so an equal amount of DMSO was added as a mock treatment for all the "no triptolide" assays. **B:** Plot of ATP hydrolysis velocity (μM of phosphate per minute) against ATP (μM) using data from (A). GraphPad Prism version 10.3.1 for Windows (GraphPad Software, Boston, Massachusetts USA, www.graphpad.com) was used to perform Nonlinear regression on the Michaelis-Menten equation to fit the equation $Y = Vmax * X/(Km + X)$ to the data for the determination of V_{max} and K_m values.

We next tested the influence of triptolide on the ATP hydrolysis by archaeal XPB homologs StXPB2 and AfXPB, respectively (Fig. 3). We determined the V_{max} and K_m of 175 nM StXPB2 in the presence and absence of triptolide (Fig. 3A&B). StXPB2 has V_{max} of 2.31 μM [phosphate]/Minute and K_m of 748 μM [ATP]. The k_{cat} value was calculated to be 13.2 per minute. In the presence of 17.5 μM triptolide, the V_{max} was 2.50 μM [phosphate]/Minute with k_{cat} of 14.3 per minute while the K_m was 1064 μM [ATP]. These results indicate that triptolide has no significant impact on the ATP hydrolysis by StXPB2.

Similarly, triptolide has no statistically significant inhibition on the ATP hydrolysis by AfXPB (Fig. 3C&D). The V_{max} of 1.0 μM AfXPB in the absence of triptolide was determined to be 0.63 μM [phosphate]/Minute with k_{cat} of 0.63 per minute, while in the presence of 0.10 mM triptolide, it was 0.65 μM [phosphate]/Minute with k_{cat} of 0.65 per minute. The K_m for AfXPB was estimated to be 282 μM [ATP] in the absence of triptolide and 306 μM [ATP] in the presence of 0.10 mM triptolide, respectively.

Finally, we examined if triptolide inhibits the ATP hydrolysis by the StXPB2-Bax1 complex or the AfXPB-Bax1 complex (Fig. 4). Archaeal XPB homologs are usually associated with a nuclease named Bax1 to form a helicase-nuclease dimer presumably to coordinate DNA damage unwinding and excision ([18]. In the absence of triptolide, the V_{max} for the StXPB2-Bax1 complex was 3.79 μM [phosphate]/Minute with k_{cat} of 25.4 per minute (Fig. 4B). In comparison, the V_{max} for the AfXPB-Bax1 complex was 0.87 μM [phosphate]/Minute with k_{cat} of 2.90 per minute (Fig. 4D). In the presence of 100x triptolide, the V_{max} values for both complexes remain almost the same, respectively, indicating that triptolide has practically no impact on the ATP hydrolysis by the archaeal XPB-Bax1 complexes. In addition, these results suggest that Bax1 stimulates the ATP hydrolysis by ~2-

fold for StXPB2 (k_{cat} of 13.2 per minute) and ~5-fold for AfXPB (k_{cat} of 0.63 per minute), respectively, in agreement with previous observations [19]. Interestingly, this extra 3-fold stimulation by AfBax1 comes from the enhancement on ATP binding to AfXPB as suggested by the Km changes between AfXPB (1232 μM [ATP], Table1) and the AfXPB-Bax1 complex (282 μM [ATP], Table 1). This is consistent with structural analyses on AfXPB and StXPB2. AfXPB was reported to stay in a stable open inactive conformation, while StXPB2 exists in multiple closed to partially opened conformations [18]. The results presented here suggest that AfBax1 stimulates the change of the open AfXPB conformation to a closed AfXPB conformation.

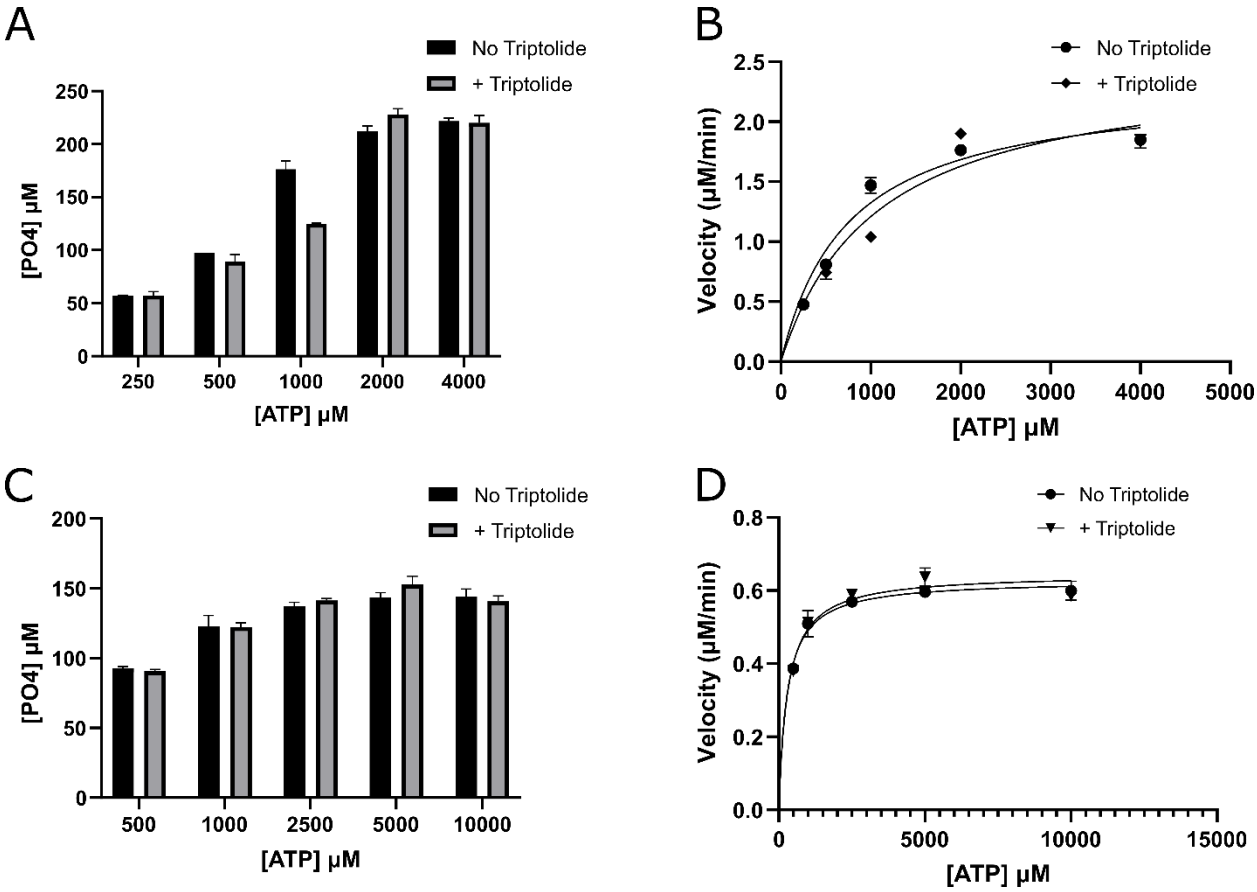

Figure 3. Triptolide has no inhibition on the ATP hydrolysis by archaeal StXPB2 or AfXPB. **A:** Phosphate produced from ATP hydrolysis by 0.175 μM StXPB2 with 0.438 μM ssDNA oligomer in the presence and absence of 17.5 μM triptolide over a range of ATP concentrations from 250 to 4000 μM. Data are mean ± standard deviation from triplicate measurements carried out at 50 ^{0}C for 2 hours as described in the methods. **B:** Plot of ATP hydrolysis velocity (μM of phosphate per minute) against ATP (μM) using data from (A). **C:** Phosphate produced from ATP hydrolysis by 1.0 μM AfXPB with 2.5 μM ssDNA oligomer in the presence and absence of 0.10 mM triptolide over ATP concentrations ranging from 0.5 to 10 mM. Data are mean ± standard deviation from triplicate measurements carried out at 50 ^{0}C for 4 hours as described in the methods. **D:** Plot of ATP hydrolysis velocity (μM of phosphate per minute) against ATP (μM) using data from (C). Velocity plots are prepared in the same way as described in Fig. 2B.

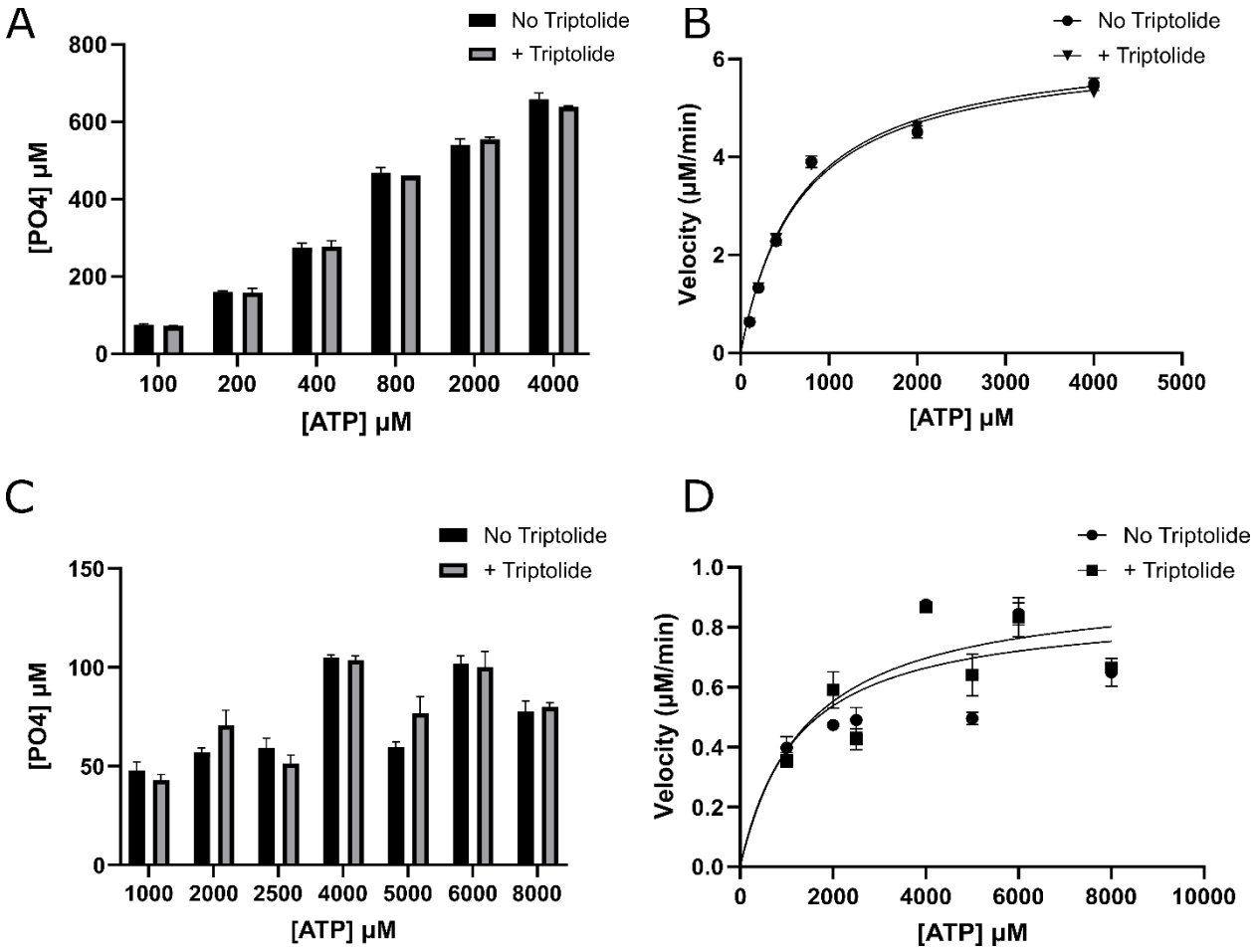

Figure 4. The impact of triptolide on the ATP hydrolysis by archaeal XPB-Bax1 complexes. A: Phosphate produced from the ATP hydrolysis by 0.125 µM the StXPB2-Bax1 complex with 0.350 µM ssDNA oligomer in the presence and absence of 12.5 µM triptolide. Data are mean ± standard deviation from triplicate measurements carried out at 50 ^{0}C for 2 hours as described in the methods. B: Plot of ATP hydrolysis velocity (µM of phosphate per minute) against ATP (µM) using data from (A). C: Phosphate produced from the ATP hydrolysis by 0.30 µM the AfXPB-Bax1 complex with 0.750 µM ssDNA oligomer in the presence and absence of 30 µM triptolide. Data are mean ± standard deviation from triplicate measurements carried out at 50 ^{0}C for 2 hours as described in the methods. D: Plot of ATP hydrolysis velocity (µM of phosphate per minute) against ATP (µM) using data from (C). Velocity plots are prepared in the same way as described in Fig. 2B.

Table 1. List of k_{cat} and Km values for all the tested enzymes

Enzymes		k_{cat} (min^{-1})		Km (µM [ATP])	
Name	Concentration (uM)	No Triptolide	+ Triptolide	No Triptolide	+ Triptolide
AfXPB-Bax1	0.300	2.90	3.13	282	306
AfXPB	1.000	0.63	0.65	1232	1420
StXPB2-Bax1	0.250	25.40	25.04	1059	1188
StXPB2	0.175	13.20	14.29	748	1064
HsXPB	0.050	44.20	15.00	1083	546

2.2 Computational analyses of the interactions of triptolide with XPB

To further investigate the binding of triptolide to XPB, triptolide was docked to HsXPB (PDB ID: 7NVV) [20], and its archaeal homologs AfXPB (PDB ID: 2FWR) and StXPB2 (PDB ID: 6P4F) using AutoDock4 [21]. The detected triptolide-binding sites are ranked by Autosite score. Autosite score is a geometry-based score and favors binding sites with many points in compact buried cavities [22]. Table 2 summarizes the top 5 binding sites ranked by Autosite score for triptolide to bind HsXPB, StXPB2, and AfXPB.

Table 2. Top 5 Binding sites detected by AutoSite for HsXPB, StXPB2, and AfXPB.

Enzyme	Site	Autosite score	Points	RadGyr	Buriedness
HsXPB	1	48.88	326	5.30	0.89
	2	45.65	340	6.01	0.90
	3	35.18	130	3.66	1.00
	4	34.96	208	4.60	0.88
	5	26.28	116	3.27	0.86
StXPB2	1	49.36	261	4.06	0.88
	2	32.53	257	5.32	0.82
	3	29.13	193	4.30	0.81
	4	26.81	125	3.93	0.92
	5	22.69	154	5.01	0.86
AfXPB	1	25.96	221	5.80	0.83
	2*	13.77	55	2.56	0.80
	3	13.13	20	1.40	0.96
	4	12.37	52	2.40	0.76
	5	11.92	21	1.44	0.90

*The original top 2 binding site on AfXPB is too tiny to accommodate triptolide. In addition, triptolide bound to this site is disastrously unfavorable, with many clashes identified in the AMBER and CHARMm forcefields (not shown). So, this site is removed from the list, and all subsequent site numbers are increased by one. The score for pocket ranking is calculated by multiplying the fill size (number of points) by the square of its buriedness and then dividing this product by the radius of gyration. Buriedness is determined by the ratio of grid points tagged as buried to the total surface area grid points. This scoring method prioritizes fills that are large in volume and have compact, buried cavities [22].

The spatial distribution of predicted triptolide-binding sites is illustrated in Figure 5, demonstrating distinct binding site configurations across homologs of the XPB protein. For human XPB (HsXPB), the top five binding sites predominantly cluster around the helicase domain 1 (HD1) (Fig. 5, left), with binding site 2 uniquely positioned in the groove between HD1 and HD2 near the ATP-binding site. Conversely, in Sulfolobus tokodaii XPB (StXPB2), these binding sites are distributed more remotely from HD1 (Fig. 5, middle). Specifically, binding sites 4 and 5 are in the groove between HD1 and DRD, while sites 1 and 3 are positioned in the groove bridging HD1 and HD2, and the remaining site lies near the ThM domain.

Unlike both HsXPB and StXPB2, the XPB homolog in Archaeoglobus fulgidus (AfXPB) exhibits an open conformation, wherein the groove between HD1 and HD2 is entirely exposed. The key triptolide binding sites in AfXPB are consolidated between the helicase domains within this open configuration (Fig. 5, right). These findings underscore the variability in triptolide-binding site arrangements among the XPB homologs, revealing that triptolide's binding mechanism is non-conserved [9,18].

Analysis of Autosite scoring reveals a hierarchical significance of binding pockets. On HsXPB, binding pockets ranked 1 and 2 appear distinctively more prominent than other identified sites, whereas, on AfXPB and StXPB2, the top-ranking binding pockets exhibit exceptional scores (Table 2). The functional roles of these binding sites are explored further, particularly in the context of their potential to mediate interactions with other

proteins or DNA. For instance, mutations in regions associated with XPB's interaction with p52 or p8 confer resistance to triptolide inhibition, implicating these interfaces in XPB's triptolide sensitivity. Similarly, alterations in DNA-binding residues have also been linked to triptolide resistance, as evidenced by prior studies [23].

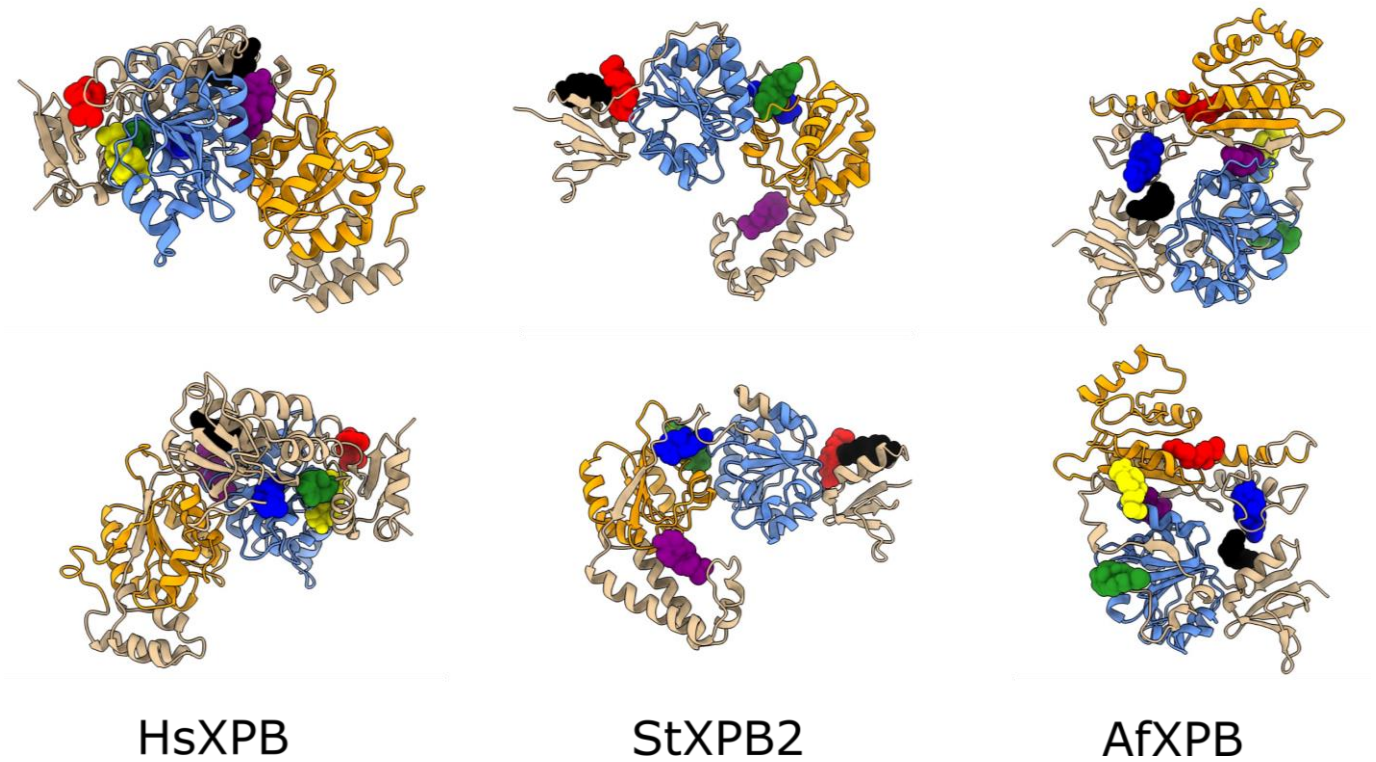

Figure 5. Distribution of the top binding sites ranked by Autosite for triptolide on HsXPB, StXPB2, and AfXPB. The front (top) and back (bottom) views of XPB protein structures in ribbons. The helicase domains 1 and 2 are highlighted in light blue and golden yellow, respectively. The three XPB structures have HD1 oriented in the same way. The top 5 or 6 binding sites are indicated by space-filled triptolide in different colors: Binding Site 1 – Dark Blue, Binding Site 2 – Purple, Binding Site 3 – Green, Binding Site 4 – Red, Binding Site 5 – Yellow, Binding Site 6 – Magenta.

2.2.1 Interactions of triptolide with HsXPB

Binding site 1 is located at the groove between HD1 and HD2 but away from the ATP-binding site. (Fig. 6) This binding site is mainly formed by residues Pro486, Asn481, Tyr121, Val478, Ile477, Leu 470, Lys487, Glu105, Lys117, Thr119, and Ser122 (Fig. 6). Much of the triptolide molecule, except for portions of the B & C ring and the 7,8-epoxide, is in contact with the binding pocket (Fig. 6, right). Lys117 can interact with the hydroxyl oxygen at C14 of triptolide by acting as a hydrogen bond donor with the closest amine hydrogen about 2.7 Angstroms away from the hydroxyl oxygen. Glu105 can interact with the same hydroxyl hydrogen by functioning as a hydrogen bond acceptor with the closest oxygen 2.81 Angstroms away from the hydrogen (Fig. 6, middle). Tyr121 and Val478 both interact with the isopropyl group in this pose, Tyr121 by a pi-alkyl interaction and Val478 by an alkyl interaction. In addition, Lys487 is engaged in an alkyl interaction with the A ring and the carbonyl of the peptide backbone of Ile477 is engaged in a carbon hydrogen bond with the D ring (Fig. 6, middle). Binding Site 1 had an affinity score of -8.51kcal/mol in the best pose detected by AutoDock4.

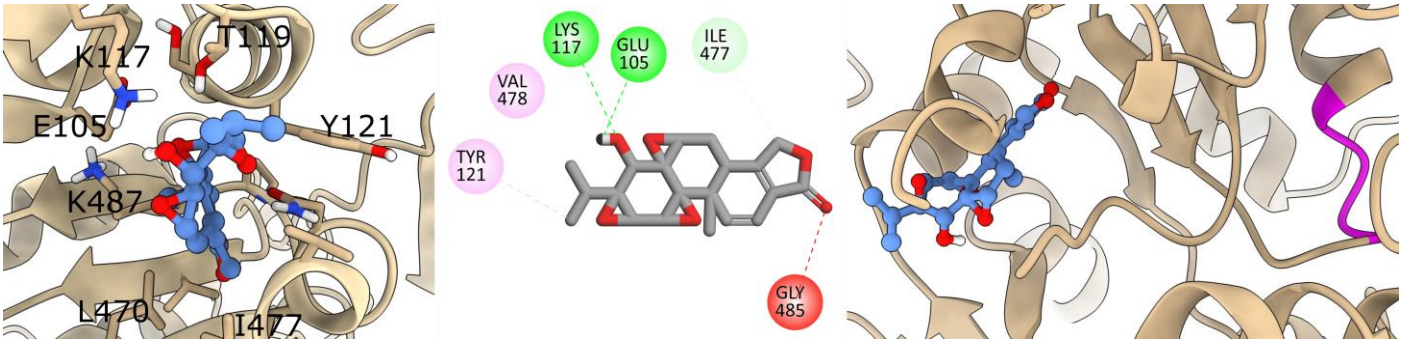

Figure 6. The interactions of triptolide and HsXPB at binding site 1. Left: the location of binding site 1 in 3D representation using the AMBER forcefield. Important pocket residues are labeled; middle: 2D representation using the CHARMM forcefield of the interacting residues at binding site 1. Conventional hydrogen bonds are represented in bright green, carbon-hydrogen bonds in light green, alkyl interactions in pink, alkyl-pi interactions are pink with a dotted line, and unfavorable interactions are indicated in red; right: 3D representation showing the docked triptolide in blue and the Walker A motif in magenta.

Binding site 2 consists of residues Trp381, Leu348, Gln320, Arg317, Lys346, Ser347, Gln377, Arg645, Cys342, Gln373, Arg642, Gly345, Ala344, Gly343, and Asp616 (Fig. 7).

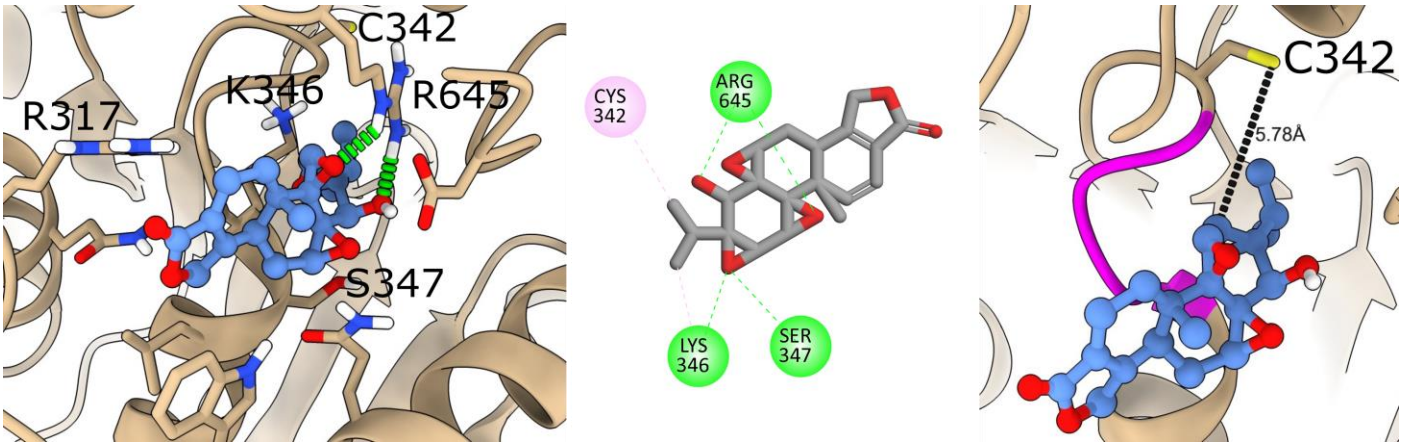

Figure 7. The interactions of triptolide and HsXPB at binding site 2. Left: the location of binding site 1 in 3D representation using the AMBER forcefield. Important pocket residues are labeled; middle: 2D representation using the CHARMM forcefield of the interacting residues at binding site 1. Conventional hydrogen bonds are represented in bright green, carbon-hydrogen bonds in light green, alkyl interactions in pink, alkyl-pi interactions are pink with a dotted line, and unfavorable interactions are indicated in red; right: 3D representation showing the docked triptolide in blue and the Walker A motif in magenta.

Binding site 2 overlaps with and occludes the Walker A motif. (Fig. 7, right) The binding of triptolide at site 2 seems likely to cause ATPase inhibition. Much of the triptolide molecule, except for the A ring, is in contact with HsXPB (Fig. 7). Two possible hydrogen bonds were identified between triptolide (the hydroxyl oxygen at C14 and the 12,13-epoxide oxygen) and the guanidinium group of Arg645 (Fig. 7, middle). The bond length from the 12,13-epoxide oxygen to the secondary amine of the arginine guanidinium group is 2.06 angstroms in this pose. In addition, residues Lys346 and Ser347 from the Walker A motif also have traditional hydrogen bond interactions with the 12-13 epoxide, and Lys346 was also found to have alkyl interactions with the isopropyl group.

Interestingly, residue Cys342, which was previously reported to be covalently cross-linked with triptolide through the 12-13 epoxide [9], is oriented towards carbon 12 and 13 of triptolide, the cysteine beta carbon is 4.40 Angstroms away from the isopropyl group. Using the rotamer in the PDB 7NVV model, the sulfur of Cys342 is just over 5.00

Angstroms away from the isopropyl group. Changing the rotamer to a different one in the Dunbrack library can decrease the distance to 3.91 Angstroms [24]. When this rotamer is applied, the sulfur of Cys342 is 5.78 Angstroms from Carbon-12 with which it is proposed to react (Fig 7, right). Binding site 2 had an affinity score of -7.32 kcal/mol in the best pose detected by AutoDock4. For comparison, triptolide was covalently crosslinked to XPB by creating a bond between the 12-carbon and the sulfur of Cys342, simulating a nucleophilic attack on the 12-carbon resulting in ring opening of the 12,13-epoxide. When constrained by this covalent bond, the optimal pose identified by ADFR to covalently link triptolide with residue Cys342 of HsXPB had an affinity of -2.8 kcal/mol. However, it is relevant to mention that ADFR, used for covalent docking experiments, limits the number of residues within the structure that can be treated as flexible. It seems likely that the affinity score could be improved via the reorientation of sidechains that form the binding pocket and nearby molecular surface since there were more residues capable of interacting with triptolide than our system could compute simultaneously. The irreversible linking of triptolide to Cys342 will inhibit the ATPase activity of HsXPB. This agrees with the results of He and colleagues [8,9].

Binding site 3, with buriedness score of 1.0, is completely buried within the protein and has no access to solvent. Analysis of the model in ChimeraX confirmed this (not shown). Triptolide could not likely have access to this site without significant conformational changes in HsXPB.

Binding site 4 is composed of residues Glu434, His461, His172, Lys171, Lys167, Arg332, Asp296, Asp300, Ser301, Val302, Glu178, Val169, Leu170, Tyr295, and Asn303 (Fig. 8). The isopropyl group, the 12,13-epoxide, the hydroxyl, the 9,11-epoxide, the methyl group, as well as portions of the A ring and the butenolide all have contacts with HsXPB in this pose. The carbonyl of the butenolide group forms three hydrogen bonds to the two primary amines of Arg332 and the amine of Lys167 (Fig. 8, middle). Two histidine residues, His461 and His172, are involved in pi-alkyl interactions with the isopropyl group of triptolide. Lys171 and Val302 have alkyl interactions with the isopropyl group. Binding site 4 had an affinity score of -7.45 kcal/mol in the best pose detected by AutoDock4.

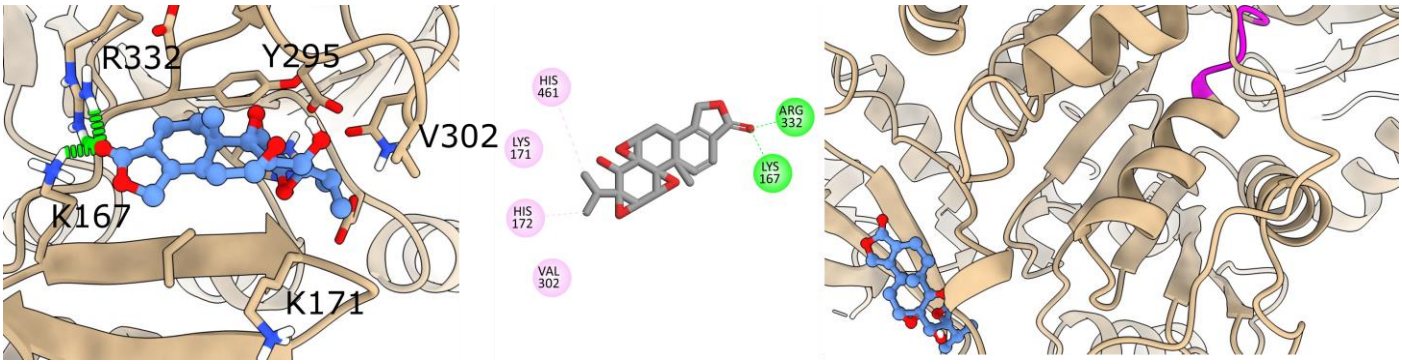

Figure 8. The interactions of triptolide and HsXPB at binding site 4. Left: the location of binding site 4 in 3D representation using the AMBER forcefield. Important pocket residues are labeled; middle: 2D representation using the CHARMM forcefield of the interacting residues at binding site 4. Conventional hydrogen bonds are represented in bright green, carbon-hydrogen bonds in light green, alkyl interactions in pink, alkyl-pi interactions are pink with a dotted line, and unfavorable interactions are indicated in red; right: 3D representation showing the docked triptolide in blue and the Walker A motif in magenta.

Binding site 5 was defined by residues Tyr489, Lys322, Pro318, Tyr319, Tyr501, Leu496, Asn499, Glu495, Asn492, Gln97, Val101, Asp98, Arg109, Glu490, and Ala491 (Fig. 9). The entire triptolide molecule, except for portions of the A & B rings, is in contact with the binding pocket in this pose. Three hydrogen bonds were identified. One from the butenolide carbonyl to Tyr501, one from the 8,7-epoxide to the peptide backbone, and one

from the 12,13-epoxide to the amine of Lys322. Additionally, Tyr489 is in a pi-alkyl interaction with the isopropyl group and Val101 is in an alkyl interaction with the isopropyl group. Ala491 and Leu496 are in alkyl interactions with the B ring. Binding site 5 had an affinity score of -8.21 kcal/mol in the optimal pose of triptolide detected by AutoDock4 for this site.

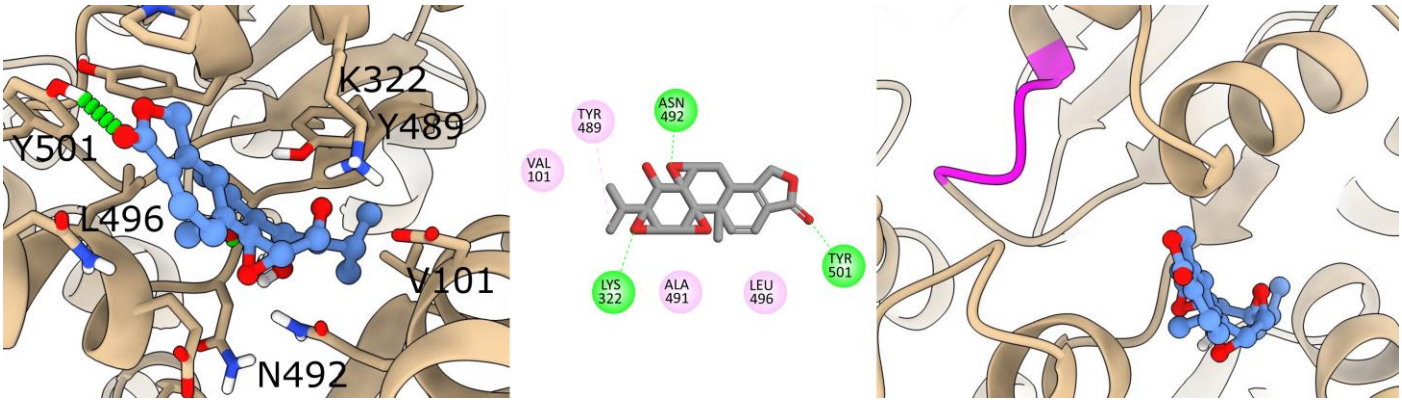

Figure 9. The interactions of triptolide and HsXPB at binding site 5. Left: the location of binding site 5 in 3D representation using the AMBER forcefield. Important pocket residues are labeled; middle: 2D representation using the CHARMM forcefield of the interacting residues at binding site 5. Conventional hydrogen bonds are represented in bright green, carbon-hydrogen bonds in light green, alkyl interactions in pink, alkyl-pi interactions are pink with a dotted line, and unfavorable interactions are indicated in red; right: 3D representation showing the docked triptolide in blue and the Walker A motif in magenta.

In summary, detailed structural analyses on the top 5 binding sites predicted by AutoDock4 for HsXPB indicate that binding site 2 will likely inhibit ATPase activity due to its proximity to the Walker A motif. Additionally, because other sites with similar affinity to binding site 2 were identified, triptolide may bind to HsXPB at more than one position.

2.2.2 Interactions of triptolide with StXPB2

Binding site 1 is defined by Thr92, Pro91, Ala94, Arg409, Leu411, Arg412, Leu420, Leu419, Ala418, Lys238, Tyr237, Lys236, Ala235, Ile234, Tyr233, Gly408, Ile239, Gly93, and Glu227 (Fig. 10). This binding site is located near the Walker A motif (Fig 10) but does not overlap with it in agreement with our ATPase assay that ATPase inhibition is not observed when triptolide binds to this site (Fig. 3). Two hydrogen bonds to the peptide backbone were detected (Fig. 10, middle). One from the carbonyl oxygen of the butenolide to the amide bond between Tyr237 and Lys238 and the other from the 9,11-epoxide oxygen to the amide bond between Ile234 and Ala235. Ala94, Pro91, and Arg412 are all involved in alkyl interactions with the isopropyl group. Ile234, Leu411, and Ala418 are involved in alkyl interactions with the A ring, and Ile234 is additionally engaged in an alkyl interaction with the B ring. Only a portion of the B ring in triptolide is not in contact with StXPB2. Binding site 1 had an affinity score of -8.92 kcal/mol for the best pose with triptolide.

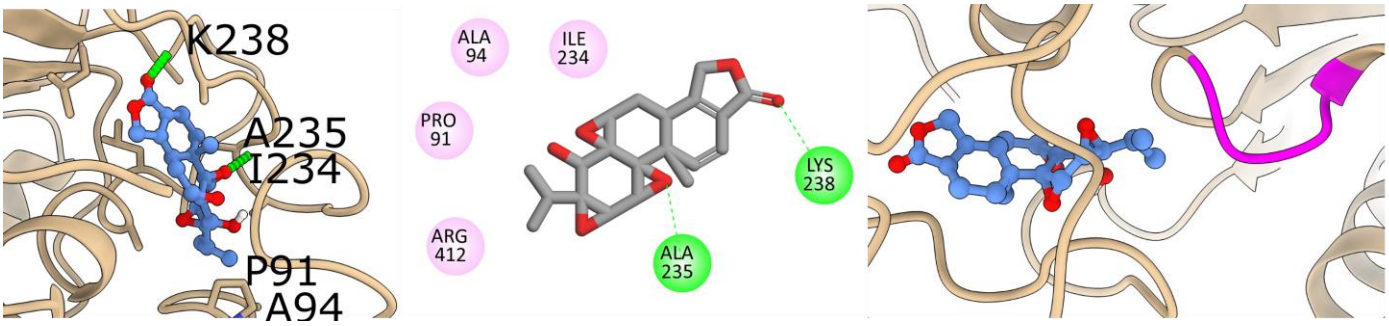

Figure 10. The interactions of triptolide and StXPB2 at binding site 1. Left: the location of binding site 1 in 3D representation using the AMBER forcefield. Critical pocket residues are labeled; middle: 2D representation using the CHARMM forcefield of the interacting residues at binding site 1. Conventional hydrogen bonds are represented in bright green, carbon-hydrogen bonds in light green, alkyl interactions in pink, alkyl-pi interactions are pink with a dotted line, and unfavorable interactions are indicated in red; right: 3D representation showing the docked triptolide in blue and the Walker A motif in magenta.

2.2.3 Interactions of triptolide with AfXPB

Binding site 1 is formed by residues Glu69, Arg298, Leu297, Trp323, Lys305, Phe289, Ile295, Tyr286, Thr296, and Lys287 (Fig. 11). Much of the triptolide molecule, except for portions of the A & B rings, is in contact with the receptor (Fig. 15, right). Several hydrogen bonds were identified (Fig. 11, middle). The 7,8-epoxide makes two hydrogen bonds to the protein's peptide backbone involving Leu297 and Arg298. The 12,13-epoxide makes a hydrogen bond with the amine of Lys287 at 2.182 angstroms. The amine group of Lys305 is engaged in a hydrogen bond with the carbonyl of the butenolide moiety at 1.710 angstroms. The alpha carbon of Thr296 is involved in a carbon-hydrogen bond with the 9,11-epoxide moiety. Phe289 and Tyr286 are involved in pi-alkyl interactions with the A ring. Additionally, Lys 287 is participating in alkyl interactions with the A & B rings. The isopropyl group is primarily solvent-exposed but does participate in an alkyl interaction with Leu297 (Fig. 11, middle). Binding site 1 had an affinity score of -6.58 kcal/mol in the best-docked pose of triptolide detected by AutoDock4.

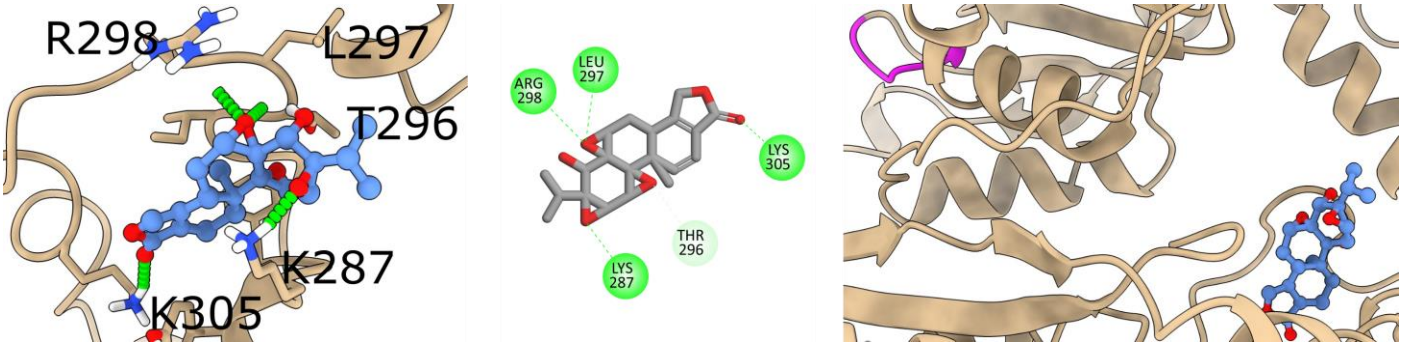

Figure 11. The interactions of triptolide and AfXPB at binding site 1. Left: the location of binding site 1 in 3D representation using the AMBER forcefield. Critical pocket residues are labeled; middle: 2D representation using the CHARMM forcefield of the interacting residues at binding site 1. Conventional hydrogen bonds are represented in bright green, carbon-hydrogen bonds in light green, alkyl interactions in pink, alkyl-pi interactions are pink with a dotted line, and unfavorable interactions are indicated in red; right: 3D representation showing the docked triptolide in blue and the Walker A motif in magenta.

3. Materials and Methods

3.1 Docking

In silico, solvent docking was performed using AutoDock4 (https://AutoDock4.scripps.edu) [21] to interrogate potential triptolide binding sites on HsXPB (PDB ID: 7NVV), AfXPB (PDB ID: 2FWR). and StXPB2 (PDB ID: 6P4F). Before the molecular docking, these PDB coordinates were pretreated to remove all water molecules, nonstandard residues, and all other protein and peptide chains from the model except for XPB. Then, all hydrogens, including implicit hydrogens, were added to the structure. Next, nonpolar hydrogens were merged with their parent atom. Finally, Kollman charges were added to the model. The prepared model was loaded into AGFR 1.0, and Autosite 1.0 (https://ccsb.scripps.edu/autosite/) [22] was used to compute ligand binding pockets. The

highest-scoring binding sites detected by Autosite 1.0 for these XPB orthologs were further analyzed in Discovery Studio (https://discover.3ds.com/discovery-studio-visualizer-download), AutoDock4, and ChimeraX (https://www.cgl.ucsf.edu/chimerax/) [25].

3.2 *Covalent Docking of triptolide to HsXPB*

Covalent docking of triptolide with HsXPB was undertaken based on reports in the literature of a covalent adduct formed between the 12,13-epoxide of triptolide and Cys342 [9]. To evaluate this binding site in silico AutoDock4 for Flexible Receptors (ADFR) was used. ADFR is a program that can be used for covalent docking and can also specify that some sidechains remain flexible rather than rigid, as all sidechains are in AutoDock4 [21,26]. This analysis showed that triptolide's best pose, while covalently crosslinked, resulted in an affinity score of -2.8 kcal/mol. This agrees with the conclusions of He and colleagues, namely that there is a thermodynamically favorable binding site on XPB when triptolide is covalently crosslinked at the 12-carbon to Cys342 of HsXPB [9].

3.3 *AI Docking of triptolide to XPB*

Artificial Intelligence, known as AI, is an emerging technology. It has been adapted to numerous tasks with considerable fanfare. Some groups have applied AI to molecular simulations and docking. One such application is AlphaFold3 (https://alphafold-server.com/), which can dock common ligands such as ATP to protein structures. Comparing the docking of ATP by AlphaFold3 to HsXPB with a crystal structure containing ADP, we found that AlphaFold3 was capable of docking ATP to the phosphate-binding Walker A motif, in agreement with the crystal structure (PDB ID 7NVV).

Another commercial AI tested for docking capabilities was Balto (https://balto.deeporigin.io/chat). In the AI's own words, Balto's purpose is to "assist with tasks related to Chemistry, Biology, and Drug Discovery." By initiating a simple, text-based chat with Balto, we retrieved PDB files, generated structures from SMILES for triptolide, and performed docking using Deep Origin's proprietary algorithm. Balto automatically detected binding pockets and docked triptolide to the Walker A motif of HsXPB (7NVV) (not shown) [27].

3.4 *ATPase Assay*

The ATPase activity was monitored using an endpoint assay that measures the amount of inorganic phosphate liberated by enzyme-catalyzed hydrolysis of ATP during a reaction containing ATP and an ATPase enzyme. ATPase reactions were carried out as previously described [17] in an ATPase reaction buffer containing 50mM HEPES pH 8.2, 100mM KCl, 5mM MgCl2, 1mM dithiothreitol (DTT) with appropriate ATP, and a single-stranded (ss) DNA oligomer (5'-ACAGCATGTGATCGATAGTCTCTAG-3') with specified concentrations in the figure legends. HsXPB was co-expressed as an XPB-p52-p8 trimer in Sf9 cells. AfXPB and StXPB2 (XPB2) were prepared as recombinant proteins from E. coli.

3.5 *Statistical Analysis*

To determine if the differences between ATPase enzyme velocity in the presence or absence of triptolide were significant, a comparison of fits was performed using GraphPad Prism version 10.3.1 for Windows (GraphPad Software, Boston, Massachusetts USA, www.graphpad.com). All outliers were removed from data sets by the Grubbs test [28].

4. Conclusions

In this study, we examined the interactions between triptolide, a potent natural anticancer agent, and the XPB protein, comparing its effects on human XPB (HsXPB) and archaeal homologs AfXPB and StXPB2. Triptolide demonstrated a specific inhibitory effect on the ATPase activity of HsXPB but did not impact the archaeal homologs, underscoring a lack of conservation in its interaction across XPB variants. Computational docking revealed distinct spatial distributions of triptolide-binding sites among these homologs,

with binding affinities and structural dynamics that further supported the differential inhibitory activity.

We have modeled the covalent binding of triptolide to the residue Cys342 near the phosphate-binding Walker A motif of HsXPB. This interaction partially overlaps with the phosphate-binding motif and involves residues such as Lys346, Gly343, and Cys342, indicating that triptolide obstructs ATP hydrolysis by physically occluding the Walker A motif. In contrast, the archaeal homologs lack this critical cysteine residue, instead possessing a threonine substitution, which prevents covalent binding and explains the absence of inhibitory activity. These findings align with prior mutagenesis studies showing that substitutions at Cys342 abrogate triptolide's inhibitory effects [9,23].

Our investigation also identified a potential two-step binding mechanism for triptolide on HsXPB. In this model, triptolide first associates with a higher-affinity non-covalent site (site 2), positioning it for a nucleophilic attack on the 12-carbon by the sulfur of Cys342. This leads to the formation of a covalent adduct, shifting triptolide to a lower affinity but thermodynamically stable binding pocket, effectively locking the molecule in place and ensuring sustained inhibition of ATPase activity. Indeed, a two-step mechanism is common among irreversible inhibitors that are at least partially selective for their target [29].

This study highlights the specificity of triptolide's inhibitory mechanism and provides a structural basis for its selective activity against HsXPB. By elucidating the critical role of residue Cys342 and the structural differences among XPB homologs, our findings pave the way for rational drug design efforts to improve triptolide's selectivity and reduce off-target effects. Future studies could explore synthetic derivatives targeting the conserved elements of the Walker A motif to expand therapeutic applications while minimizing toxicity.

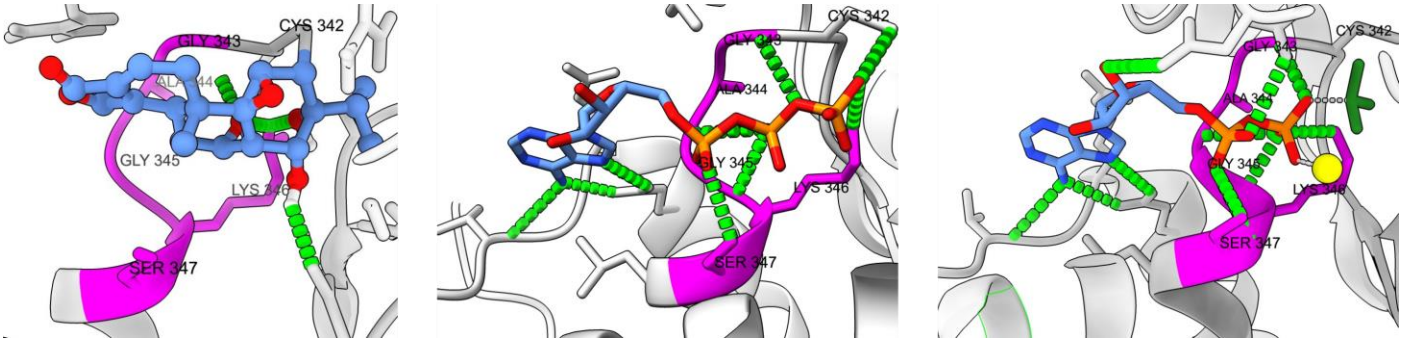

Figure 12. Covalently-crosslinking of Triptolide with Cys342 blocks ATP hydrolysis by HsXPB. Left: Triptolide (in blue) was covalently docked into HsXPB structure (PDB ID: 7NVV) by cross-linking C12 of triptolide with S of Cys342 residue using AutoDock4FR; middle: ATP docking to HsXPB sequence using AlphaFold3; right: HsXPB with bound ADP-BeF3 (PDB ID: 7NVV). Green dashed lines indicate predicted hydrogen bonds, and the phosphate-binding Walker A motif is magenta. This image clearly shows that the covalent binding of triptolide at this site occludes the phosphate-binding Walker A motif.

Author Contributions: Conceptualization, D.G..; methodology, D.G.; validation, D.G.; formal analysis, D.G.; investigation, D.G.; data curation, D.G.; writing—original draft preparation, D.G.; writing—review and editing, D.G., visualization, D.G., Funding: This research was partially funded by the UCR Committee on Research Grant.

Data Availability Statement: The original contributions presented in the study are included in the article/supplementary material; further inquiries can be directed to the corresponding author.

Acknowledgments: D.G. thanks Marco Bravo for reading the manuscript and having helpful discussions.

Conflicts of Interest: The author declares no conflict of interest. The funders had no role in the study's design, data collection, analysis, interpretation, manuscript writing, or decision to publish the results.

References

1. Kupchan, S.; Court, W.; Dailey, R.J.; Gilmore, C.; Bryan, R. Triptolide and tripdiolide, novel antileukemic diterpenoid triepoxides from Tripterygium wilfordii. *Journal of American Chemical Society* **1972**, *94*, 7194–7195, doi:10.1021/ja00775a078.
2. Zhou, Z.L.; Yang, Y.X.; Ding, J.; Li, Y.C.; Miao, Z.H. Triptolide: structural modifications, structure-activity relationships, bioactivities, clinical development and mechanisms. *Nat Prod Rep* **2012**, *29*, 457-475, doi:10.1039/c2np00088a.
3. Tong, L.; Zhao, Q.; Datan, E.; Lin, G.Q.; Minn, I.; Pomper, M.G.; Yu, B.; Romo, D.; He, Q.L.; Liu, J.O. Triptolide: reflections on two decades of research and prospects for the future. *Nat Prod Rep* **2021**, *38*, 843-860, doi:10.1039/d0np00054j.
4. Cui, D.; Xu, D.; Yue, S.; Yan, C.; Liu, W.; Fu, R.; Ma, W.; Tang, Y. Recent advances in the pharmacological applications and liver toxicity of triptolide. *Chem Biol Interact* **2023**, *382*, 110651, doi:10.1016/j.cbi.2023.110651.
5. Chen, S.R.; Dai, Y.; Zhao, J.; Lin, L.; Wang, Y.; Wang, Y. A Mechanistic Overview of Triptolide and Celastrol, Natural Products from Tripterygium wilfordii Hook F. *Front Pharmacol* **2018**, *9*, 104, doi:10.3389/fphar.2018.00104.
6. Gao, J.; Zhang, Y.; Liu, X.; Wu, X.; Huang, L.; Gao, W. Triptolide: pharmacological spectrum, biosynthesis, chemical synthesis and derivatives. *Theranostics* **2021**, *11*, 7199-7221, doi:10.7150/thno.57745.
7. Manzo, S.G.; Zhou, Z.L.; Wang, Y.Q.; Marinello, J.; He, J.X.; Li, Y.C.; Ding, J.; Capranico, G.; Miao, Z.H. Natural product triptolide mediates cancer cell death by triggering CDK7-dependent degradation of RNA polymerase II. *Cancer Res* **2012**, *72*, 5363-5373, doi:10.1158/0008-5472.CAN-12-1006.
8. Titov, D.V.; Gilman, B.; He, Q.L.; Bhat, S.; Low, W.K.; Dang, Y.; Smeaton, M.; Demain, A.L.; Miller, P.S.; Kugel, J.F.; et al. XPB, a subunit of TFIIH, is a target of the natural product triptolide. *Nat Chem Biol* **2011**, *7*, 182-188, doi:10.1038/nchembio.522.
9. He, Q.L.; Titov, D.V.; Li, J.; Tan, M.; Ye, Z.; Zhao, Y.; Romo, D.; Liu, J.O. Covalent modification of a cysteine residue in the XPB subunit of the general transcription factor TFIIH through single epoxide cleavage of the transcription inhibitor triptolide. *Angew Chem Int Ed Engl* **2015**, *54*, 1859-1863, doi:10.1002/anie.201408817.
10. Hoag, A.; Duan, M.; Mao, P. The role of Transcription Factor IIH complex in nucleotide excision repair. *Environ Mol Mutagen* **2023**, doi:10.1002/em.22568.
11. Moreland, R.J.; Tirode, F.; Yan, Q.; Conaway, J.W.; Egly, J.M.; Conaway, R.C. A role for the TFIIH XPB DNA helicase in promoter escape by RNA polymerase II. *J Biol Chem* **1999**, *274*, 22127-22130, doi:10.1074/jbc.274.32.22127.
12. Wang, R.; Sun, Y.; Li, C.; Xue, Y.; Ba, X. Targeting the DNA Damage Response for Cancer Therapy. *Int J Mol Sci* **2023**, *24*, doi:10.3390/ijms242115907.
13. Jiang, S.; Wan, F.; Lian, H.; Lu, Z.; Li, X.; Cao, D.; Jiang, Y.; Li, J. Friend or foe? The dual role of triptolide in the liver, kidney, and heart. *Biomed Pharmacother* **2023**, *161*, 114470, doi:10.1016/j.biopha.2023.114470.
14. Li, Z.; Zhou, Z.L.; Miao, Z.H.; Lin, L.P.; Feng, H.J.; Tong, L.J.; Ding, J.; Li, Y.C. Design and synthesis of novel C14-hydroxyl substituted triptolide derivatives as potential selective antitumor agents. *J Med Chem* **2009**, *52*, 5115-5123, doi:10.1021/jm900342g.
15. Xu, H.; Tang, H.; Feng, H.; Li, Y. Design, synthesis and anticancer activity evaluation of novel C14 heterocycle substituted epi-triptolide. *Eur J Med Chem* **2014**, *73*, 46-55, doi:10.1016/j.ejmech.2013.11.044.
16. Xu, F.; Shi, X.; Li, S.; Cui, J.; Lu, Z.; Jin, Y.; Lin, Y.; Pang, J.; Pan, J. Design, synthesis, and biological evaluation of novel water-soluble triptolide derivatives: Antineoplastic activity against imatinib-resistant CML cells bearing T315I mutant Bcr-Abl. *Bioorg Med Chem* **2010**, *18*, 1806-1815, doi:10.1016/j.bmc.2010.01.052.
17. Lanzetta, P.A.; Alvarez, L.J.; Reinach, P.S.; Candia, O.A. An improved assay for nanomole amounts of inorganic phosphate. *Anal Biochem* **1979**, *100*, 95-97, doi:10.1016/0003-2697(79)90115-5.
18. Rouillon, C.; White, M.F. The XBP-Bax1 helicase-nuclease complex unwinds and cleaves DNA: implications for eukaryal and archaeal nucleotide excision repair. *J Biol Chem* **2010**, *285*, 11013-11022, doi:10.1074/jbc.M109.094763.

19. Ma, X.; Hong, Y.; Han, W.; Sheng, D.; Ni, J.; Hou, G.; Shen, Y. Single-stranded DNA binding activity of XPBI, but not XPBII, from Sulfolobus tokodaii causes double-stranded DNA melting. *Extremophiles* **2011**, *15*, 67-76, doi:10.1007/s00792-010-0338-z.
20. Aibara, S.; Schilbach, S.; Cramer, P. Structures of mammalian RNA polymerase II pre-initiation complexes. *Nature* **2021**, *594*, 124-128, doi:10.1038/s41586-021-03554-8.
21. Morris, G.M.; Huey, R.; Lindstrom, W.; Sanner, M.F.; Belew, R.K.; Goodsell, D.S.; Olson, A.J. AutoDock4 and AutoDockTools4: Automated docking with selective receptor flexibility. *J Comput Chem* **2009**, *30*, 2785-2791, doi:10.1002/jcc.21256.
22. Ravindranath, P.A.; Sanner, M.F. AutoSite: an automated approach for pseudo-ligands prediction-from ligand-binding sites identification to predicting key ligand atoms. *Bioinformatics* **2016**, *32*, 3142-3149, doi:10.1093/bioinformatics/btw367.
23. Smurnyy, Y.; Cai, M.; Wu, H.; McWhinnie, E.; Tallarico, J.A.; Yang, Y.; Feng, Y. DNA sequencing and CRISPR-Cas9 gene editing for target validation in mammalian cells. *Nat Chem Biol* **2014**, *10*, 623-625, doi:10.1038/nchembio.1550.
24. Shapovalov, M.V.; Dunbrack, R.L., Jr. A smoothed backbone-dependent rotamer library for proteins derived from adaptive kernel density estimates and regressions. *Structure* **2011**, *19*, 844-858, doi:10.1016/j.str.2011.03.019.
25. Meng, E.C.; Goddard, T.D.; Pettersen, E.F.; Couch, G.S.; Pearson, Z.J.; Morris, J.H.; Ferrin, T.E. UCSF ChimeraX: Tools for structure building and analysis. *Protein Sci* **2023**, *32*, e4792, doi:10.1002/pro.4792.
26. Ravindranath, P.A.; Forli, S.; Goodsell, D.S.; Olson, A.J.; Sanner, M.F. AutoDockFR: Advances in Protein-Ligand Docking with Explicitly Specified Binding Site Flexibility. *PLoS Comput Biol* **2015**, *11*, e1004586, doi:10.1371/journal.pcbi.1004586.
27. Garik Petrosyan, G.P., Natalie Ma, Tigran Abramyan. We Spill the Beans: Deep Origin's AI- and Physics-Based Models for Drug Discovery. **2024**, *2024*.
28. Organisation, I.S. *ISO 5725-2, Application of Statistics – Accuracy (Trueness and Precision) of MeasurementMethods and Results – Part 2: Basic Method for the Determination of Repeatability and Reproducibility of a Standard Measurement Method*; 1994.
29. Copeland, R.A. *Evaluation of Enzyme Inhibitors in Drug Discovery: A Guide for Medicinal Chemists and Pharmacologists*, 2nd ed.; John Wiley & Sons, Inc.: 2013.